Anticancer Nanoparticles

Deutsche Ausgabe: DOI: 10.1002/ange.201506115
Internationale Ausgabe: DOI: 10.1002/anie.201506115

Near-Infrared-Activated Nanocalorifiers in Microcapsules: Vapor Bubble Generation for In Vivo Enhanced Cancer Therapy

Jingxin Shao, Mingjun Xuan, Luru Dai, Tieyan Si, Junbai Li, and Qiang He**

Abstract: *Photothermal therapy based on gold nanostructures has been widely investigated as a state-of-the-art noninvasive therapy approach. Because single nanoparticles cannot harvest sufficient energy, self-assemblies of small plasmonic particles into large aggregates are required for enhanced photothermal performance. Self-assembled gold nanorods in lipid bilayer-modified microcapsules are shown to localize at tumor sites, generate vapor bubbles under near-infrared light exposure, and subsequently damage tumor tissues. The polyelectrolyte multilayer enables dense packing of gold nanorods during the assembly process, which leads to the formation of vapor bubbles around the excited capsules. The resulting vapor bubbles achieve a high efficiency of suppressing tumor growth compared to single gold nanorods. In vivo experiments demonstrated the ability of soft-polymer multilayer microcapsules to cross the biological barriers of the body and localize at target tissues.*

Photothermal therapy (PTT) has increasingly become an inexpensive and facile oncological treatment method because of its spatial and temporal selectivity and minimal invasiveness.[1] Among the common photothermal conversion agents, plasmonic gold nanostructures, which can efficiently convert adsorbed photons into thermal energy, have received great attention.[2–4] It is well-known that near-infrared (NIR) light can easily penetrate into living organisms with minimally invasive effects.[3] In particular, gold nanorods (GNRs) have been extensively explored in the field of PTT, in part because of their strong absorption in the NIR region.[1] Also, GNRs exhibit faster and higher heating effects compared to other gold materials since they have higher intrinsic absorption efficiencies.[5] Previous studies have shown that light-activated GNRs not only bring heat, but also generate vapor nanobubbles (VNBs), depending on the laser power used.[6] Direct heating leads to thermal ablation of cancer cells and subsequent cell death. Interestingly, VNB generation can cause local mechanical damage instead of harming the surrounding healthy tissue.[7–9] GNRs in early clinical studies have shown some promise in cancer PTT treatment.[10,11] However, heat converted by dispersed GNRs is often insufficient to damage the tumor tissues in practice.[12] Therefore, it is highly desirable to develop supramolecular aggregates of plasmonic GNRs to obtain optimal photothermal conversion efficiency for enhanced PTT, which subsequently can be disassembled into smaller discrete GNRs and rapidly cleared by the immune system.

In the last two decades, layer-by-layer (LbL) assembled polyelectrolyte microcapsules have been widely recognized as a cell-mimicking drug carrier.[13,14] Recent studies have shown that those soft polyelectrolyte multilayer microcapsules can exhibit similar deformability like that of red blood cells (RBCs) by using a microfluidic blood capillary model that mimics dimensions and pressure differentials of the in vivo environment.[15] To the best of our knowledge, to date no in vivo environments have been shown to support these microcapsules.

In this work, we report a novel design of biocompatible GNR-assembled chitosan (CHI)/sodium alginate (ALG) microcapsules with biomimetic surface modifications composed of L-α-phosphatidylcholine (L-PC), L-α- phosphatidic acid (L-PA), and 1,2-distearoyl-*sn*-glycero-3-phosphoethanolamine-*N*-[folate(polyethylene glycol)-2000] (folate-DSPE) as an enhanced photothermal antitumor platform (Supporting Information, Figure S1). Briefly, CHI, ALG, and GNRs were used as materials to construct microcapsules by using LbL assemblies according to previously reported procedures.[16] GNR-$(CHI/ALG)_5$ microcapsules were further modified with fluid lipid bilayers composed of L-PC, L-PA, DSPE-PEG_{2000}, and folate-DSPE, which can be performed by using a vesicle fusion method.[17,18] Under NIR laser irradiation, vapor bubbles can be generated around excited GNR-$(CHI/ALG)_5$ capsules. In vitro experiments show that the resulting vapor bubbles could selectively damage tumor cells in a short time. In vivo experiments further confirm that this $(CHI/ALG)_5$ capsule-based antitumor system can effectively localize at tumor sites owing to its deformability and molecule recognition between the folate group and the receptor overexpressed by the tumor cells.[19] Furthermore, theoretical simulations show that assembled GNRs are required to produce enough heat for VNBs generation.

GNR-$(CHI/ALG)_5$ capsules were prepared by using LbL assembly as reported previously.[20] The typical transmission

[*] J. Shao, M. Xuan, Dr. T. Si, Prof. Q. He
Key Lab for Microsystems and Microstructures Manufacturing, Micro/Nanotechnology Research Center, Harbin Institute of Technology
Yikuangjie 2, Harbin 150080 (China)
E-mail: qianghe@hit.edu.cn
Dr. L. Dai
Key Lab for Biomedical Effects of Nanomaterials and Nanosafety, National Center for Nanoscience and Technology
Beiyitiao 11, ZhongGuanCun, Beijing 100190 (China)
Prof. J. Li
Beijing National Laboratory for Molecular Sciences (BNLMS), Key Laboratory of Colloid and Interface Science, Institute of Chemistry, Chinese Academy of Sciences
Beiyijie 2, ZhongGuanCun, Beijing 100190 (China)
E-mail: jbli@iccas.ac.cn

Supporting information for this article is available on the WWW under http://dx.doi.org/10.1002/anie.201506115.

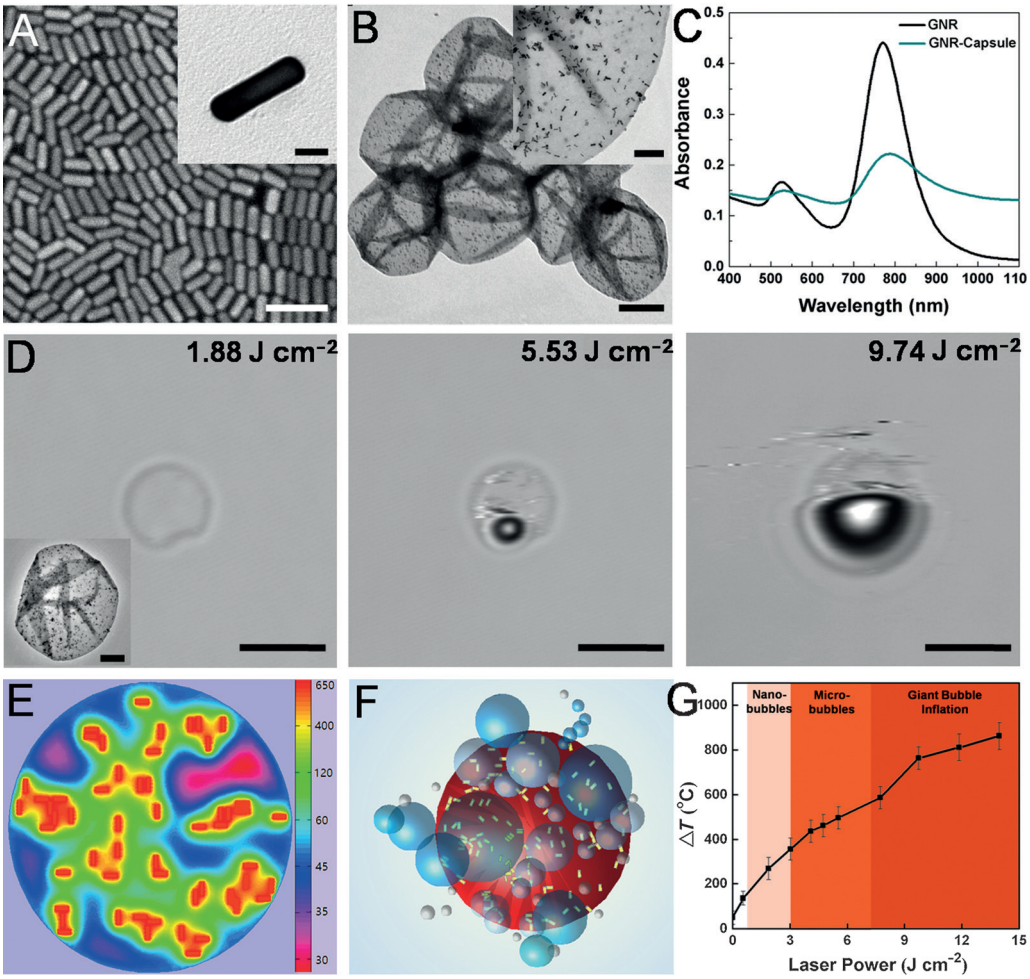

Figure 1. A) SEM image of the gold nanorods (GNRs). Scale bar: 100 nm. Inset: enlarged TEM image of a single GNR (scale bar: 20 nm). B) TEM image of $(CHI/ALG)_5$ capsules (scale bar: 2 μm). Inset: higher-magnification TEM image of a single capsule (scale bar: 500 nm). C) UV/Vis-NIR extinction spectra of GNRs (black line) and GNR-$(CHI/ALG)_5$ capsules (blue line). D) TP-CLSM images of aqueous GNR-$(CHI/ALG)_5$ capsule solution irradiated by using a 808 nm NIR laser with laser fluence of 1.88 J cm^{-2}, 5.53 J cm^{-2} and 9.74 J cm^{-2}, respectively. Scale bar: 5 μm. Inset: TEM image of a single GNR-$(CHI/ALG)_5$ capsule (scale bar: 1 μm). E) Theoretical simulation of the elevated profile of temperature after NIR irradiation with a laser fluence of 5.53 J cm^{-2} (corresponding to the inset TEM image in Figure 1 D). The color bar represents the increase of temperature (°C). F) Illustration of vapor microbubble emergence around GNR-capsules under NIR irradiation. G) Theoretical computation of the relationship between the increase of temperature and NIR power used. The colored regions correspond to different thermophysical responses.

electron microscopy (TEM) image in Figure 1 A shows that the GNRs have an aspect ratio of 3.9 and an average length of 54.2 ± 1.3 nm. The negatively charged GNRs at 4 mg mL^{-1} was assembled into the wall of $(CHI/ALG)_5$ capsules through electrostatic attractions. Both scanning electron microscopy (SEM; Figure S2) and TEM (Figure 1 B) images show that the GNRs have successfully assembled into the wall of capsules. The inset TEM image with higher magnification in Figure 1 B demonstrates the uniform distribution of GNRs in the wall of capsules with a density of about 66 ± 5 particles μm^{-2}. The density of assembled GNRs in the capsules rises linearly with increasing GNR concentration below 4 mg mL^{-1} (Figure S3 A), but is roughly constant above 4 mg mL^{-1}. The UV/Vis-NIR absorption spectrum of GNR-$(CHI/ALG)_5$ capsules in Figure 1 C has the maximum absorption peak at 780 nm, exhibiting a slight red shift compared to that of the GNRs.[21–23] We used this characteristic surface plasmon resonance (SPR) adsorption to test their photothermal effects and study vapor bubble generation.

Figure 1 D shows the two photon confocal laser scanning microscopy (TP-CLSM) images of a GNR-$(CHI/ALG)_5$ capsule irradiated by an NIR laser. It can be seen that no vapor microbubbles were observed around the capsule upon NIR irradiation at the lowest laser fluence tested (1.88 J cm^{-2}). Once the laser fluence was increased to 5.53 J cm^{-2}, a vapor microbubble appeared on one side of the excited GNR-$(CHI/ALG)_5$ capsule. When the laser fluence was further increased to 9.74 J cm^{-2}, a larger vapor microbubble rapidly formed. The vapor bubble formation can be explained by GNRs on the wall of $(CHI/ALG)_5$ capsules converting adsorbed photons into thermal energy and thus superheating water around the capsules. Here, the heat transfer equation was employed to theoretically compute the stable spatial distribution of temperature for the excited GNRs in the wall of capsules upon NIR irradiation with a laser power of 5.53 J cm^{-2} (corresponding to the TEM image of Figure 1 B). The temperature contours around GNRs of capsules in Figure 1 E were obtained by solving the heat transfer equation according to previously reported procedures.[24] The highest temperature covers the whole length of the GNRs in the equatorial plane passing the central axis of the cylinder. The anisotropic temperature profile is most obvious in a circle with a radius of 60 nm. In the region far away from the center of the GNRs, the temperature profile becomes spherically symmetric. This highly confined heat distribution has been also confirmed by other theoretical simulations.[25] Figure 1 F illustrates the formation of VNBs around the surface of

microcapsules, showing that the generated VNBs around the GNRs form larger vapor bubbles on the surface of microcapsules. Furthermore, several studies have demonstrated that there was a laser power threshold for the formation of VNBs on different gold nanostructures, because local temperature must be higher than the critical temperature of the surrounding medium.[26–28] With increasing laser fluence, photothermal conversion results in a rapid temperature increase according to the above calculation as shown in Figure 1G. The size and lifetime of vapor bubbles are proportional to the laser fluence. Hence, different stages of bubble formation should exist, including VNBs,[29] microbubbles, and giant bubbles, depending on the used NIR laser fluence. However, VNBs are currently difficult to observe because of their extremely small size and short lifetime. Note that bubble generation is also dependent on the density of assembled GNRs in the capsules. Figure S3B demonstrates that vapor bubbles could only be observed when the GNRs concentration exceeds 3 mg mL^{-1} at a laser fluence of 5.53 J cm^{-2}.

To test laser-induced microbubble generation in biological medium, three groups of MCF-7 cells were incubated with GNR-(CHI/ALG)$_5$ capsules for 30 min, and then free capsules were removed. The bright-field TP-CLSM images in Figure 2 show a high targeting adhesion of the capsules on the surfaces of MCF-7 cells owing to the specific recognition ability of folate groups. Next, cells were irradiated for 5 min by using an NIR laser fluence of 1.88 J cm^{-2}, 5.53 J cm^{-2}, and 9.74 J cm^{-2}. The corresponding videos can be obtained in the Supporting Information (Videos S1-S3). Note that propidium iodide (PI) is here used as a fluorescence indicator to stain dead cells since PI is membrane-impermeable and is generally excluded from viable cells. Time-lapsed bright-field TP-CLSM images in Figure 2A show no vapor microbubble generation upon irradiation at the lowest laser fluence (1.88 J cm^{-2}). Also, no red fluorescence in the PI channel was observed, indicating that the irradiated MCF-7 cells are still alive, similar to those in the absence of GNR-(CHI/ALG)$_5$ capsules (Figure S4). When the used laser fluence was increased to 5.53 J cm^{-2}, vapor microbubbles became visible with increasing irradiation time (Figure 2B). Correspondingly, time-lapsed images in the PI channel show that the nuclei of cancer cells around the capsules rapidly displayed red fluorescence owing to the diffusion of PI dyes into the cells, demonstrating that these cells have died. The rapid expansion of the bubble volume resulted in tearing and destroying the tumor cells. This means that the cell-damage mechanism is mainly based on the mechanical destruction associated with the formation of explosive vapor microbubbles. It is dramatically different from the heating damage mechanism observed for other photothermal agents based on monodisperse gold nanoparticles or carbon nanotubes. When the stronger laser fluence (9.74 J cm^{-2}) was applied, larger vapor microbubbles formed and cell necrosis occurred faster (Figure 2C), indicating that the efficiency of the collective heating effect was linearly-dependent upon laser power. These results are consistent with our theoretical computations (Figure 1G) that the size of a vapor bubble can be tuned easily by the incident laser fluence. Meanwhile, in the corresponding control groups, all MCF-7 cells irradiated by using the laser fluence above the threshold of vapor microbubble generation did not display red fluorescence in the absence of GNR-(CHI/ALG)$_5$ capsules (Figures S5, S6), indicating that laser irradiation alone is not able to kill tumor cells. Cell viability was further evaluated by a standard 3-(4,5-dimethylthiazol-2-yl)-2,5-diphenyltetrazolium bromide (MTT) assay (Figure S7). Compared to control groups, cell necrosis was significantly observed in the experimental group where cells were first incubated with capsules and then exposed under NIR laser for 5 min, with a cell viability

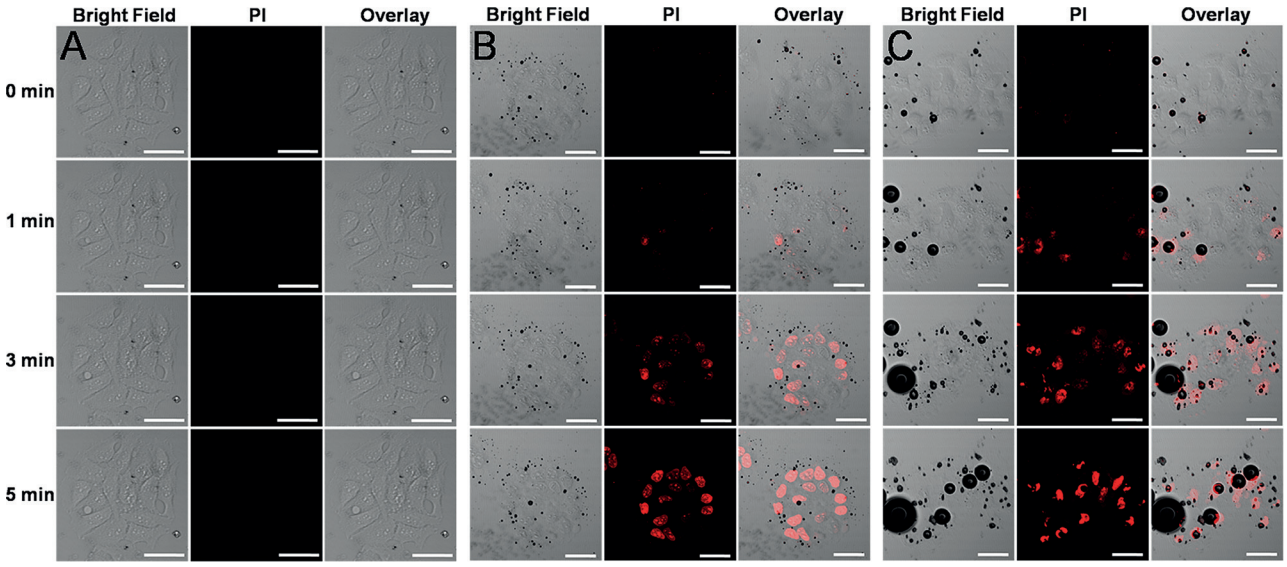

Figure 2. Time-lapsed TP-CLSM images of MCF-7 cells loaded with GNR-(CHI/ALG)$_5$ capsules in the presence of propidium iodide (PI) fluorochrome irradiated by a 808 nm NIR laser with different fluence: A) 1.88 J cm^{-2}, no vapor bubbles were observed. B) 5.53 J cm^{-2}, small vapor bubbles appeared with the appearance of red fluorescence on the cells. The red fluorescence means that cell necrosis occurred and the PI probe could enter into cells. C) 9.74 J cm^{-2}, giant bubbles were quickly generated with the cell necrosis. Scale bars: 50 μm.

decrease of about 60-65%. Finally, the biocompatibility of GNR-$(CHI/ALG)_5$ capsules was assessed by the MTT assay (Figure S8). The cell viability did not significantly decrease with increasing concentration of capsules, and exhibited negligible toxicity to NIH/3T3 cells.

On the basis of the in vitro vapor bubble-enhanced PTT effect, we first investigated the feasibility of using the GNR-$(CHI/ALG)_5$ capsules for in vivo PTT in a mouse model bearing 4T1 tumors. To monitor the distribution of GNR-$(CHI/ALG)_5$ capsules, a NIR fluorescent dye, Cyanine 7 (Cy7) with an excitated wavelength of 750 nm was used. Fluorescence images demonstrate the successful conjugation of Cy7 (Figure S9). When the tumors in mice reached a size of about 100 mm^3, 300 μL of Cy7-GNR-$(CHI/ALG)_5$ capsules solution were injected intravenously through the tail vein and then in vivo fluorescence imaging was conducted at different time points (Figure 3A). The Cy7-GNR-$(CHI/ALG)_5$ capsules tended to accumulate in the tumor site, where the Cy7 fluorescence signal showed a significant increase over time after injection. Also, strong Cy7 fluorescence signals could be observed up to 8 h post-injection, indicating that our capsules can be used for the tumor diagnosis and qualitative estimation of the tumor size. Furthermore, particles with a size of above 200 nm can efficiently activate the human complement system, and are hence rapidly cleared from the blood circulation and predominantly taken up by the reticuloendothelial system (RES) including the liver and spleen.[30,31] In contrast, RBCs can easily pass through capillaries with dimensions smaller than their size and have a long circulation time in living organisms owing in part to their deformability .[32] Recent reports have demonstrated that polymer microcapsules or hydrogel particles can behave like RBCs in a microfluidic blood capillary model mimicking in vivo biological environments.[33,34] Our capsules with diameters of 5 μm administered by intravenous tail-vein injection could accumulate in the tumor site, which should be attributed to their shape deformation like that of RBCs owing to higher osmotic pressure during blood circulation.

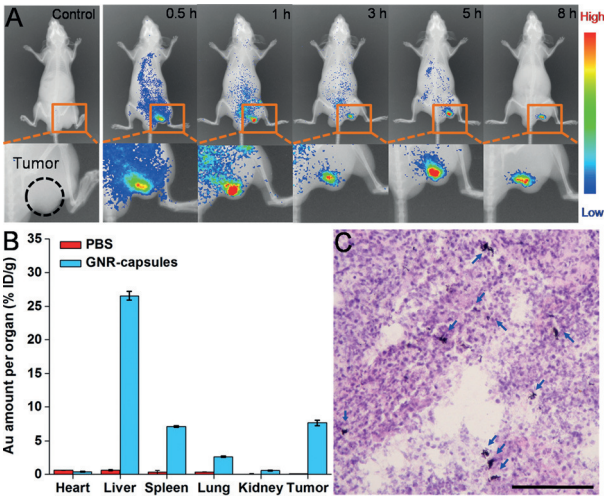

Figure 3. A) In vivo fluorescence images of the 4T1 tumor-bearing nude mouse before and after injecting Cy7-conjugated GNR-$(CHI/ALG)_5$ capsules through the tail vein. Images were taken at different time points (0.5 h, 1 h, 3 h, 5 h, 8 h). B) Biodistribution of Cy7-GNR capsules in the organ and tumor tissues harvested 24 h after capsule injection ($n=5$). C) Histology image of the tumor tissue stained by hematoxylin-eosin (HE) 24 h after the Cy7-GNR-capsule injection. The blue arrows indicate the GNRs in the capsules. Scale bar: 50 μm.

Inductively coupled plasma mass spectrometry (ICP-MS) experiments were conducted at 24 h post-injection to quantitatively measure the biodistribution of Cy7-GNR-capsules in the tumor and organs. Figure 3B shows that Au element mainly existed in the liver, spleen, and tumor. In particular, the content of Au element in the tumor was over 7.66% ID g^{-1} (injected dose per gram), indicating a higher targeting efficacy of the capsules. By staining the tissue slides with hematoxylin-eosin (HE), the capsules containing GNRs in the tumor tissues could also be visualized directly as previously reported.[35] The histology image of the HE-stained tumor tissue slide after 24 h of the injection shows some black dots (blue arrows, Figure 3C), which represent the GNRs in the capsules. Hence, these results demonstrate the accumulation of Cy7-GNR-capsules in the tumor.

Finally, we evaluated the in vivo antitumor effect of Cy7-GNR-$(CHI/ALG)_5$ capsules. Four groups of murine breast 4T1 tumor-bearing mice were used in our experiment (Figure 4). In the treatment group (capsules plus laser), mice were intravenously injected with capsules (300 μL) through the tail vein and then irradiated with an 808 nm laser at 3.83 J cm^{-2} above the threshold of photothermal bubble generation for 5 min. Other control groups of mice included PBS, GNR-capsules without laser, and mice subjected to laser irradiation only (laser only). The treatment group showed a remarkable delay in tumor growth compared to the control groups after 15 d (Figure 4A,B). All of the tumors in the treatment group were effectively ablated and only black scars were left in the original tumor sites. In contrast, the three control groups showed increasing tumor volume over time. All of the tumors were dissected and weighted after 15 d (Figure 4C). The mean tumor weight in the treatment group was notably smaller than that of three control groups. HE staining assay was performed to analyze the tumor tissues harvested from each group. Tumor tissues from the experimental group (Cy7-GNR-capsules injection and NIR irradiation) showed pronounced morphological features of cell necrosis (Figure 4D), while tumor tissues in the control groups remained intact. The toxicity was further evaluated by analyzing the tissue slices from mice administered with capsules. Compared with control groups, no obvious inflammation, cell necrosis, or apoptosis were observed in the heart, liver, spleen, lung, and kidney, which implied the absence of evident side effects (Figure S10). Also, the in vivo toxicity of capsules was estimated by monitoring the change in the weight of the mice, and no obvious side effects were revealed since high toxicity leads to drop in body weight (Figure S11). These results indicate that our capsules can be used as fluorescent and NIR-triggered thermal theranostics.

In summary, we have developed a novel theranostic platform based on biodegradable GNR-assembled biomimetic capsules for tumor imaging and enhanced photothermal

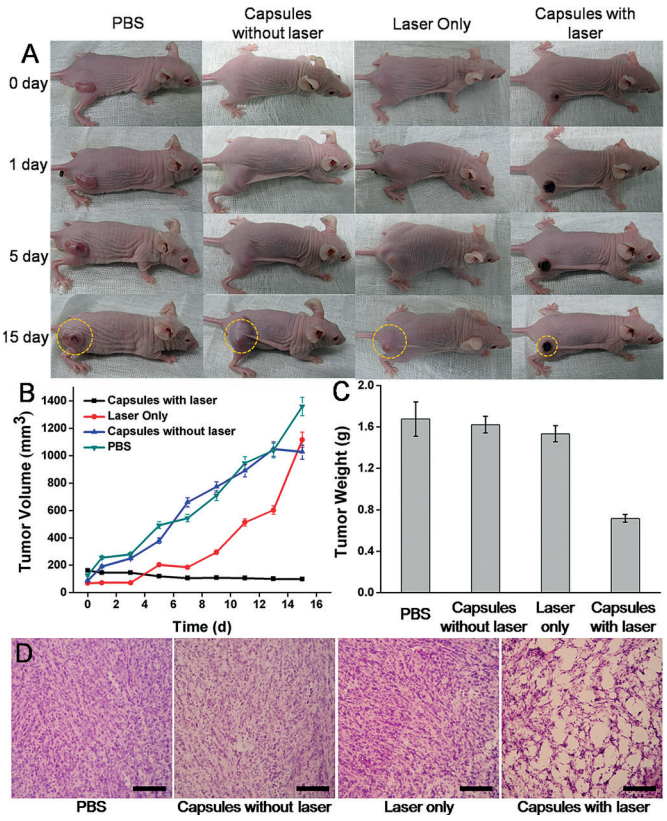

Figure 4. In vivo PTT treatment on 4T1 tumors after injection of PBS buffer, Cy7-GNR-$(CHI/ALG)_5$ capsules without laser irradiation, laser irradiation only without capsules, and capsules with laser irradiation. A) Photographs of nude mice showing the size of tumors after various treatments at different time points. B) Tumor growth curves of different groups of tumors after various treatments indicated. C) Tumor weights after 15 days. D) Histology section of the tumor tissues after 15 d h of different treatments (PBS, laser irradiation, capsules with or without NIR illumination). Scale bar: 100 μm.

treatment. Natural polyelectrolyte multilayer capsules allow dense packing of GNRs during the assembly process and then induce a collecting thermal effect between adjacent GNRs upon NIR irradiation. This leads the water around excited GNR aggregates in the capsules to form a metastable "superheated" state and thus to the formation of explosive vapor bubbles. Experimental results and theoretical simulations reveal that the explosive vapor bubbles can only be generated by using a laser fluence above 3.13 J/cm^2 (the threshold of vapor microbubble generation). The resulting photothermal vapor bubbles can locally damage tumor cells and enable PTT with high efficacy compared to single GNR as demonstrated by in vitro and in vivo experiments. Moreover, it was found that GNR-modified microcapsules delivered through tail-vein injection could successfully cross the biological barriers of the body and localize at target tissues owing to their good deformability behavior and ability, similar to that of micro-sized RBCs. This proof-of-concept study paves the way to develop explosive vapor bubble-based tumor damage for enhanced PTT.

Acknowledgements

This work was supported by the Fundamental Research Funds for the Central Universities and National Nature Science Foundation of China (21273053).

Keywords: gold nanorods · layer-by-layer · microcapsules · photothermal therapy · vapor bubbles

How to cite: *Angew. Chem. Int. Ed.* **2015**, *54*, 12782–12787
Angew. Chem. **2015**, *127*, 12973–12978

[1] L. Dykman, N. Khlebtsov, *Chem. Soc. Rev.* **2012**, *41*, 2256–2282.
[2] J. Y. Chen, D. L. Wang, J. F. Xi, L. Au, A. Siekkinen, A. Warsen, Z. Y. Li, H. Zhang, Y. N. Xia, X. D. Li, *Nano Lett.* **2007**, *7*, 1318–1322.
[3] A. G. Skirtach, A. M. Javier, O. Kreft, K. Köhler, A. P. Alberola, H. Möhwald, W. J. Parak, G. B. Sukhorukov, *Angew. Chem. Int. Ed.* **2006**, *45*, 4612–4617; *Angew. Chem.* **2006**, *118*, 4728–4733.
[4] M. Ochs, S. Carregal-Romero, J. Rejman, K. Braeckmans, S. C. De Smedt, W. J. Parak, *Angew. Chem. Int. Ed.* **2013**, *52*, 695–699; *Angew. Chem.* **2013**, *125*, 723–727.
[5] X. H. Huang, I. H. EI-Sayed, W. Qian, M. A. EI-Sayed, *J. Am. Chem. Soc.* **2006**, *128*, 2115–2120.
[6] Z. P. Qin, J. C. Bischof, *Chem. Soc. Rev.* **2012**, *41*, 1191-1217.
[7] R. H. Xiong, K. Raemdonck, K. Peynshaert, I. Lentacker, I. De Cock, J. Demeester, S. C. De Smedt, A. G. Skirtach, K. Braeckmans, *ACS Nano* **2014**, *8*, 6288–6296.
[8] A. Muñoz Javier, P. del Pino, M. F. Bedard, D. Ho, A. G. Skirtach, G. B. Sukhorukov, C. Plank, W. J. Parak, *Langmuir* **2008**, *24*, 12517–12520.
[9] D. Hühn, A. Govorov, P. R. Gil, W. J. Parak, *Adv. Funct. Mater.* **2012**, *22*, 294–303.
[10] E. B. Dickerson, E. C. Dreaden, X. H. Huang, I. H. EI-Sayed, H. H. Chu, S. Pushpanketh, J. F. McDonald, M. A. El-Sayed, *Cancer Lett.* **2008**, *269*, 57–66.
[11] W. I. Choi, A. Sahu, Y. H. Kim, G. Tae, *Ann. Biomed. Eng.* **2012**, *40*, 534–546.
[12] A. M. Alkilany, A. Shatanawi, T. Kurtz, R. B. Caldwell, R. W. Caldwell, *Small* **2012**, *8*, 1270–1278.
[13] S. Carregal-Romero, M. Ochs, W. J. Parak, *Nanophotonics* **2012**, *1*, 171–180.
[14] A. G. Skirtach, C. Dejugnat, D. Braun, A. S. Susha, A. L. Rogach, W. J. Parak, H. Möhwald, G. B. Sukhorukov, *Nano Lett.* **2005**, *5*, 1371–1377.
[15] S. P. She, C. X. Xu, X. F. Yin, W. J. Tong, C. Y. Gao, *Langmuir* **2012**, *28*, 5010-5016.
[16] E. Donath, G. B. Sukhorukov, F. Caruso, S. A. Davis, H. Möhwald, *Angew. Chem. Int. Ed.* **1998**, *37*, 2201–2205; *Angew. Chem.* **1998**, *110*, 2323–2327.
[17] Q. He, Y. Tian, H. Möhwald, J. B. Li, *Soft Matter* **2009**, *5*, 300–303.
[18] L. Duan, Q. He, K. W. Wang, X. H. Yan, Y. Cui, H. Möhwald, J. B. Li, *Angew. Chem. Int. Ed.* **2007**, *46*, 6996–7000; *Angew. Chem.* **2007**, *119*, 7126–7130.
[19] E. Forssen, M. Willis, *Adv. Drug Delivery Rev.* **1998**, *29*, 249–271.
[20] E. Donath, G. B. Sukhorukov, F. Caruso, S. A. Davis, H. Möhwald, *Angew. Chem. Int. Ed.* **1998**, *37*, 2201-2205.
[21] R. Weissleder, *Nat. Biotechnol.* **2001**, *19*, 316–317.
[22] Z. J. Zhang, J. Wang, C. Y. Chen, *Adv. Mater.* **2013**, *25*, 3869–3880.
[23] S. Nioka, B. Chance, *Technol. Cancer Res. Treat.* **2005**, *4*, 497–512.
[24] Z. G. Wu, X. K. Lin, Y. J. Wu, T. Y. Si, J. M. Sun, Q. He, *ACS Nano* **2014**, *8*, 6097–6105.

[25] I. Buttinoni, G. Volpe, F. Kümmel, G. Volpe, C. Bechinger, *J. Phys. Condens. Matter* **2012**, *24*, 284129.
[26] G. Baffou, J. Polleux, H. Rigneault, S. Monneret, *J. Phys. Chem. C* **2014**, *118*, 4890 – 4898.
[27] S. T. Wang, K. J. Chen, T. H. Wu, H. Wang, W. Y. Lin, M. Ohashi, P. Y. Chiou, H. R. Tseng, *Angew. Chem. Int. Ed.* **2010**, *49*, 3777 – 3781; *Angew. Chem.* **2010**, *122*, 3865 – 3869.
[28] V. Kotaidis, C. Dahmen, G. von Plessen, F. Springer, A. Plech, *J. Chem. Phys.* **2006**, *124*, 184702.
[29] D. Lapotko, *Nanomedicine* **2009**, *4*, 813 – 845.
[30] P. P. Adiseshaiah, J. B. Hall, S. E. McNeil, *WIREs Nanomed. Nanobiotechnol.* **2010**, *2*, 99 – 112.
[31] A. Albanese, P. S. Tang, W. C. W. Chan, *Annu. Rev. Biomed. Eng.* **2012**, *14*, 1 – 16.
[32] M. Diez-Silva, M. Dao, J. Y. Han, C. T. Lim, S. Suresh, *MRS Bull.* **2010**, *35*, 382 – 388.
[33] S. P. She, Q. Q. Li, B. W. Shan, W. J. Tong, C. Y. Gao, *Adv. Mater.* **2013**, *25*, 5814 – 5818.
[34] Q. Y. Yi, D. Y. Li, B. B. Lin, A. M. Pavlov, D. Luo, Q. Y. Gong, B. Song, H. Ai, G. B. Sukhorukov, *BioNanoSci* **2014**, *4*, 59 – 70.
[35] A. Muñoz Javier, O. Kreft, M. Semmling, S. Kempter, A. G. Skirtach, O. T. Bruns, P. del Pino, M. F. Bedard, J. Rädler, J. Käs, C. Plank, G. B. Sukhorukov, W. J. Parak, *Adv. Mater.* **2008**, *20*, 4281 – 4287.

Received: July 3, 2015
Revised: August 7, 2015
Published online: August 26, 2015